

Finite element analysis of a glass fibre reinforced composite endodontic post

A. Pegoretti*, L. Fambri, G. Zappini, M. Bianchetti

Department of Materials Engineering, University of Trento, 38050 Mesiano, Trento, Italy

Received 4 July 2001; accepted 13 November 2001

Abstract

In this work the mechanical response to external applied loads of a new glass fibre reinforced endodontic post is simulated by finite element (FE) analysis of a bidimensional model. The new post has a cylindrical shape with a smooth conical end in order to adequately fit the root cavity, and to avoid edges that could act as undesired stress concentrators. Mechanical data obtained by three-point bending tests on some prototypes fabricated in the laboratory are presented and used in the FE model. Under various loading conditions, the resulting stress component fields are hence compared with those obtained in the case of two commercial endodontic posts (i.e. a cast metal post and a carbon fibre post) and with the response of a natural tooth. The gold cast post-and-core produces the greatest stress concentration at the post-dentin interface. On the other hand, fibre-reinforced composite posts do present quite high stresses in the cervical region due to their flexibility and also to the presence of a less stiff core material. The glass fibre composite shows the lowest peak stresses inside the root because its stiffness is much similar to dentin. Except for the force concentration at the cervical margin, the glass fibre composite post induces a stress field quite similar to that of the natural tooth. © 2002 Elsevier Science Ltd. All rights reserved.

Keywords: Endodontic post; Finite element analysis; Composite materials; E-glass fibres

1. Introduction

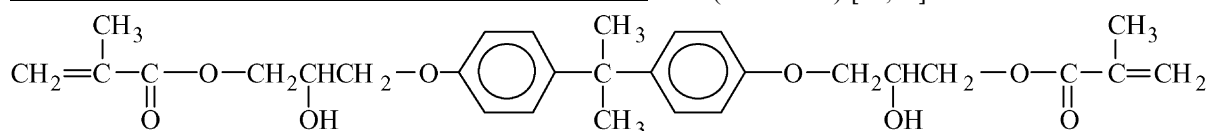
In endodontics there are mainly two classes of intervention for the treatment of pulpless teeth by using dental posts [1–4]. In the oldest one, the dentist uses a cast metal post, obtained on the basis of a mould taken from the root cavity. A cast post usually fits the root cavity in the most adequate way, since it can exactly follow its shape. More recently, prefabricated posts of various types, dimensions and materials are commercially available. The main advantage deriving from its usage is that a limited preparatory work is generally required, with a consequent saving of time and money. Although early investigations claimed that the placement of a post increases the fracture load of pulpless teeth [5–7] more recent studies failed to confirm this observation [8,9]. Important considerations can be made

by considering the materials that can be used. Cast posts are generally realised with gold alloys, while prefabricated posts can be made of various materials. In fact, stainless steel, titanium alloys, brass and zirconium oxide posts have been widely used [2,10]. In the 1990s increasing efforts were made in order to optimise the post mechanical properties for the intended application. Both dentists and producers of dental materials started to realise that the different mechanical behaviour of post and dentine is a critical parameter for the load transmission. In order to minimise the rigidity difference between the dentine and the post itself a new kind of prefabricated posts were hence developed by using polymeric composite materials [11]. A composite post commercially available under the tradename Compositopost[®], was invented by Duret et al. in 1988, and widely described in technical literature [12–18]. Compositopost[®] is made of carbon fibres embedded in an epoxy resin, and it represents the first example of this new composite post generation. More recently, a new fibre composite laminate endodontic post and core system based on a

*Corresponding author. Tel.: +39-0461-882452; fax: +39-0461-881977.

E-mail address: Alessandro.Pegoretti@ing.unitn.it (A. Pegoretti).

woven polyester bondable ribbon (Ribbon) embedded with a Bis-GMA resins was proposed by Karna [19]. Fibre-reinforced polymer composites consist of high performance fibres (i.e. fibres with elevated strength and modulus) embedded in a polymer matrix with distinct interfaces between them. They offer outstanding specific mechanical properties, corrosion resistance, impact strength, and excellent resistance under fatigue loads. An important feature of composites is that their properties can be tailored according to the particular application by varying the proportions and properties of the matrix and the reinforcement, the shape, size, orientation, and distribution of the reinforcement, and by controlling the fibre/matrix adhesion level. Mechanical response of dental posts can be experimentally investigated by suitable tests under various loading conditions [20–22]. On the other hand, more detailed information about the stress distribution surrounding endodontic posts can be evaluated by photoelastic analysis [23–26], or by numerical simulations with finite element (FE) analysis, as proposed by a number of authors [26–41], which also provides stress distribution inside the post. The FE method is based on a mathematical model which approximates the geometry



and the loading conditions of the structure (i.e. a pulpless tooth reconstructed with an endodontic post) to be analysed. Deformations and stresses in any point of the model can be evaluated and the most stressed areas can thus be evidenced [42]. Among the literature papers which we found about FE modelling of stress distributions in post and crown restored teeth [26–41], the majority of them is based on two-dimensional (2-D) models [26–34,38–41] and only few [35–37] on three-dimensional (3-D) ones. Notwithstanding the limitations related to the assumption that the stress distributions are identical in all vertical sections parallel to the selected two-dimensional model (plane strain assumption), results based on 2-D models have been widely used for modelling the clinical reality. 3-D models are surely more accurate in describing the actual state of stress but, at the same time, much more complicate to realise and they do require a much extensive computing time to be resolved. The case of maxillary central incisor with and without post restoration was recently modelled by two-dimensional (Ko et al. [33]) and three-dimensional (Ho et al. [36]) FE analysis. Despite the simplifications of the two-dimensional models, the locations of peak dentinal stresses in the two- and three-dimensional models were similar except that peak equivalent stress in the three-dimensional

model during traumatic loading was located on the facial instead of lingual dentinal surface [36].

The aim of the present work is to analyse the mechanical behaviour of a new polymeric composite post reinforced with glass fibres, both experimentally and through FE analysis. The simulation results will be compared with those of commercially available carbon fibre reinforced and gold alloy cast posts. A natural tooth restored with ideal materials, whose stiffness is equal to those of enamel and dentine, will be considered as a reference model.

2. Materials and methods

2.1. Preparation and testing of prototypes

Some cylindrical prototypes of the new glass fibre post were fabricated in the laboratory by using a pultrusion technique [43]. As a matrix we used an acrylic resin, whose main component is 2,2-bis[4-(2-hydroxy-3-methacryloyloxypropoxy)-phenyl]-propane, frequently denoted as bisphenol A glycidyl methacrylate (Bis-GMA) [10,44]:

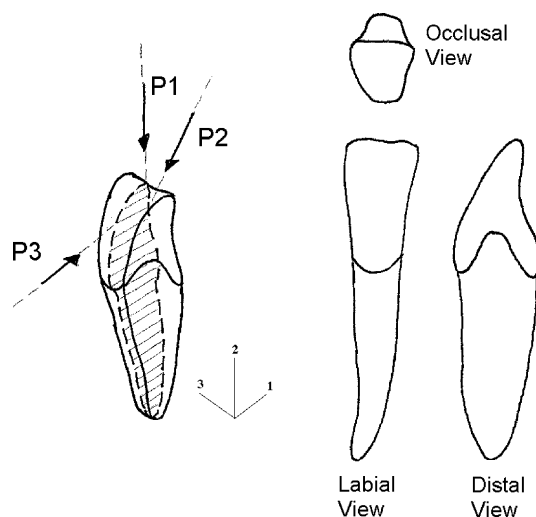


Fig. 1. Schematic of the tooth model and loading conditions, where P1 is a 100 N vertical load, P2 is a 50 N oblique (45°) load, and P3 is a horizontal 10 N load.

Reinforcement was added as unidirectional continuous *E*-glass fibres (Hybon 2001 by PPG Industries) up to a volume fraction of about 60%. Cylindrical samples with an average diameter of 1.7 ± 0.1 mm were tested in a three-point bending configuration by using an Instron 4502 testing machine equipped with a 100 N load cell. All flexural tests were carried out using a span of 40 mm (i.e. a span to depth ratio of about 23) in order to reduce shear effects to an acceptable level for the modulus measurement [45]. Tests were performed at a cross-head speed of 1 mm/min on five specimens.

2.2. FE analysis

A vertical section of an upper central incisor was bidimensionally modelled under the hypothesis of plane strain field. The model is depicted in Fig. 1: axis 1 is the labial-buccal direction, axis 2 is the occlusal direction, axis 3 is the mesio-distal direction.

With reference to Fig. 1 three different loading conditions were separately considered: P1: 100 N, vertical load, applied on the top of the crown, to simulate bruxism load [46]; P2: 50 N, oblique load, angled at 45°, to simulate the masticatory forces over lower incisors and canines; P3: 10 N, horizontal load, to simulate external traumatic forces. As a boundary

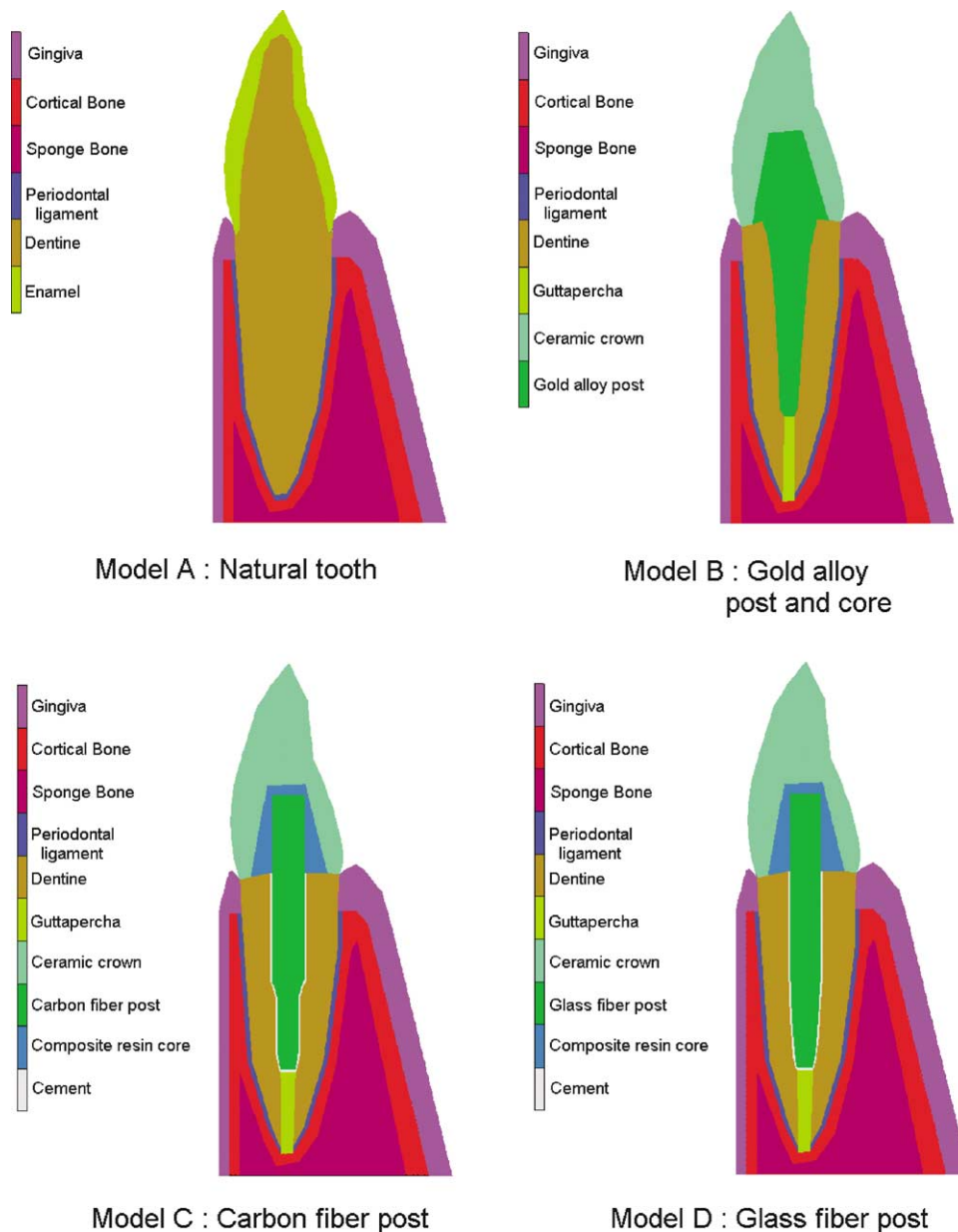


Fig. 2. Geometries and selected materials for the four different investigated models.

Table 1
Elastic properties of the isotropic materials used for the FE analysis

Material	Elastic modulus (GPa)	Poisson's coefficient
Dentine	18.6 ^a	0.31 ^a
Enamel	41.0 ^a	0.30 ^a
Periodontal ligament	68.9 × 10 ^{-3 a}	0.45 ^a
Cortical bone	13.7 ^a	0.30 ^a
Sponge bone	1.37 ^a	0.30 ^a
Gingiva	19.6 × 10 ^{-3 a}	0.30 ^a
Guttapercha	0.69 × 10 ^{-3 a}	0.45 ^a
ILOR 56 gold alloy (post-and-core)	93.0 ^b	0.33 ^c
Porcelaine (crown)	120.0 ^d	0.28 ^e
Composite resin for core built up (carbon fibre post)	3.7 ^f	0.30 ^c
Composite resin for core built up (E-glass fibre post)	7.0 ^g	0.30 ^c
Cement (carbon fibre post)	2.6 ^b	0.33 ^c
Cement (glass fibre post)	2.8 ^b	0.33 ^c

^aFrom Ko et al. [33].

^bZappini G., unpublished experimental data.

^cEstimated.

^dFrom Cavalli et al. [38].

^eFrom Pao et al. [32].

^fFrom Reynaud et al. [12].

^gZappini G., unpublished experimental data referred to Silux Plus restoration composite resin.

condition no displacements were allowed for the nodes along the bottom end line of the models. The following four different models were developed, which are schematically represented in Fig. 2 together with relative selected materials:

- **Model A:** natural tooth. It is important to observe that the root cavity was not represented. In fact, since the model is bidimensional, the root cavity would spread along the entire third dimension, while the true cavity is circular in shape, and very thin (even less than a post). In other words the model consists of a pulpless tooth restored using materials with a mechanical behaviour equal to those of enamel and dentine.
- **Model B:** pulpless tooth restored with a cast post-and-core, made of gold alloys (Ilor 56) and completed with a ceramic crown.
- **Model C:** pulpless tooth restored with a carbon fibre post Composipost[®], a composite core, and ceramic crown.
- **Model D:** pulpless tooth restored with the new glass fibre post, a composite core, and ceramic crown.

The diameter of the posts, in models B and C was the same, in order to have an identical residual dentine thickness. In the case of the cast post, an enlargement of the root cavity in the upper part was considered, like in ordinary intervention. The cement around this kind of post is usually made of zinc orthophosphate. According to Holmes et al. [39] the thickness of this cement can be estimated to be around 30 μm, and, consequently, it was not considered in the model. In restoration with

Table 2
Elastic properties for the orthotropic materials used for the FE analysis

Elastic constant	Carbon fibre post	Glass fibre post
E_L (GPa)	125 ^a	40 ^b
$E_T = E_{T'}$ (GPa)	8.5 ^a	11 ^c
$G_{LT} = G_{LT'}$ (GPa)	3.1 ^c	4.2 ^c
$G_{TT'}$ (GPa)	3.0 ^c	4.1 ^c
$\nu_{LT} = \nu_{LT'}$	0.25 ^c	0.26 ^c
$\nu_{TL} = \nu_{TL}$	0.017 ^c	0.07 ^c
$\nu_{TT'}$	0.32 ^c	0.32 ^c

^aFrom Reynaud et al. [12].

^bExperimental data.

^cTheoretical values (see Appendix A Eqs. (A.1)–(A.8)).

prefabricated post like the carbon fibre post, the thickness of the cement, which is an adhesive acrylic resin, is ranging from 100 to 250 μm. For this reason, in models C and D, a cement layer of about 200 μm was considered. All materials, except the two composite posts, were considered as homogeneous, isotropic and linear elastic, and their properties are reported in Table 1. The two composite posts were considered as linear elastic orthotropic and transversally isotropic materials and consequently five independent elastic constants are required to describe their mechanical behaviour [47]. Part of these elastic constants were obtained from direct experimental measurements, while the remaining were either taken from the literature, or estimated by appropriate theoretical formulas

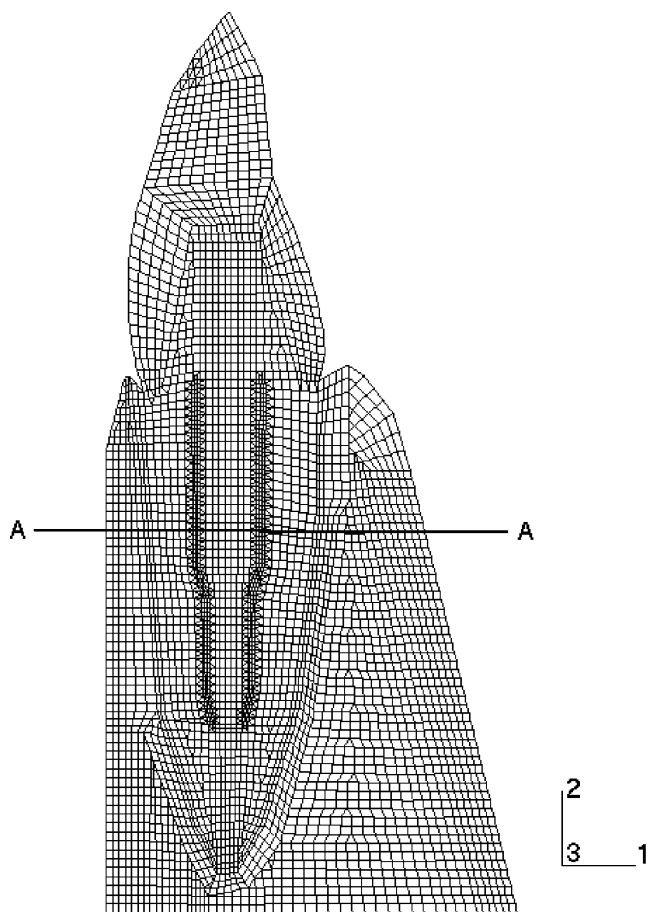


Fig. 3. FE mesh of the bidimensional model of the carbon fibre post (model C).

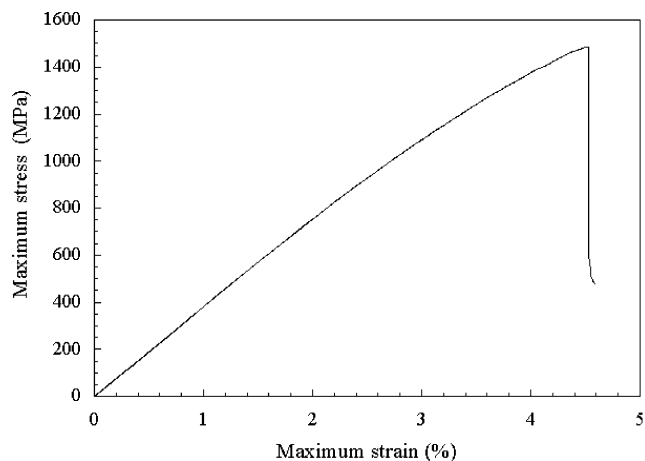


Fig. 4. Typical flexural stress–strain (evaluated in the outer layer) curve of the *E*-glass fibres composite post.

(see Appendix A). All five constants for *E*-glass and carbon fibres posts are summarised in Table 2, where *L* stands for longitudinal (parallel to fibres) direction, and

T and *T'* stand for any perpendicular direction in the transverse plane. Models A and B were composed by about 3800 nodes and 3700 elements while models C and D were composed by about 4500 nodes and 4400 elements. Most of the elements were four nodes quadrilateral and just few of them were triangular for geometrical reasons. By way of example mesh for model C is reported in Fig. 3. The commercial package Mentat™ was used to generate all FE meshes. Solution was obtained using a commercial MARC™ solving code, under license of MARC Analysis Research Corporation, Palo Alto, CA. All simulations were carried out by a Silicon Graphics (mod. Indy) workstation.

3. Results

3.1. Prototype testing

A typical plot of maximum stress versus maximum strain (i.e. stress and strain in the outer layer) of the *E*-glass composite post is reported in Fig. 4. It can be noticed that the mechanical behaviour is almost linear elastic up to fracture. Results of flexural tests performed on *E*-glass fibre reinforced post prototypes are summarised in Table 3. The longitudinal modulus, E_L , is in quite good agreement with the theoretical estimations based on the well-known rule of mixture:

$$E_L = E_f V_f + E_m (1 - V_f), \quad (1)$$

where V_f is the fibre volume fraction, E_f and E_m are the fibre and matrix elastic moduli, respectively. In fact, by considering *E*-glass fibre and matrix elastic moduli reported in Table 4, Eq. (1) yield an E_L value of about 45 GPa. It is important to observe that the composite

Table 3
Mechanical data measured on cylindrical *E*-glass fibre reinforced post prototype tested in three-point bending configuration

Modulus (GPa)	39.0 ± 2.0
Strength (MPa) (maximum stress in the outer fibres)	1390 ± 90
Maximum strain in the outer fibres (%)	4.3 ± 0.4

Table 4
Elastic constants for fibres and matrix used in Eqs. (A.1)–(A.8)

	Carbon fibres	<i>E</i> -glass fibres	Matrix
Tensile modulus, <i>E</i> (GPa)	220 (16 for <i>T</i> direction)	72.4	3.4
Shear modulus, <i>G</i> (GPa)	8.3	31	1.28
Poisson's coefficient, <i>v</i>	0.2	0.18	0.33

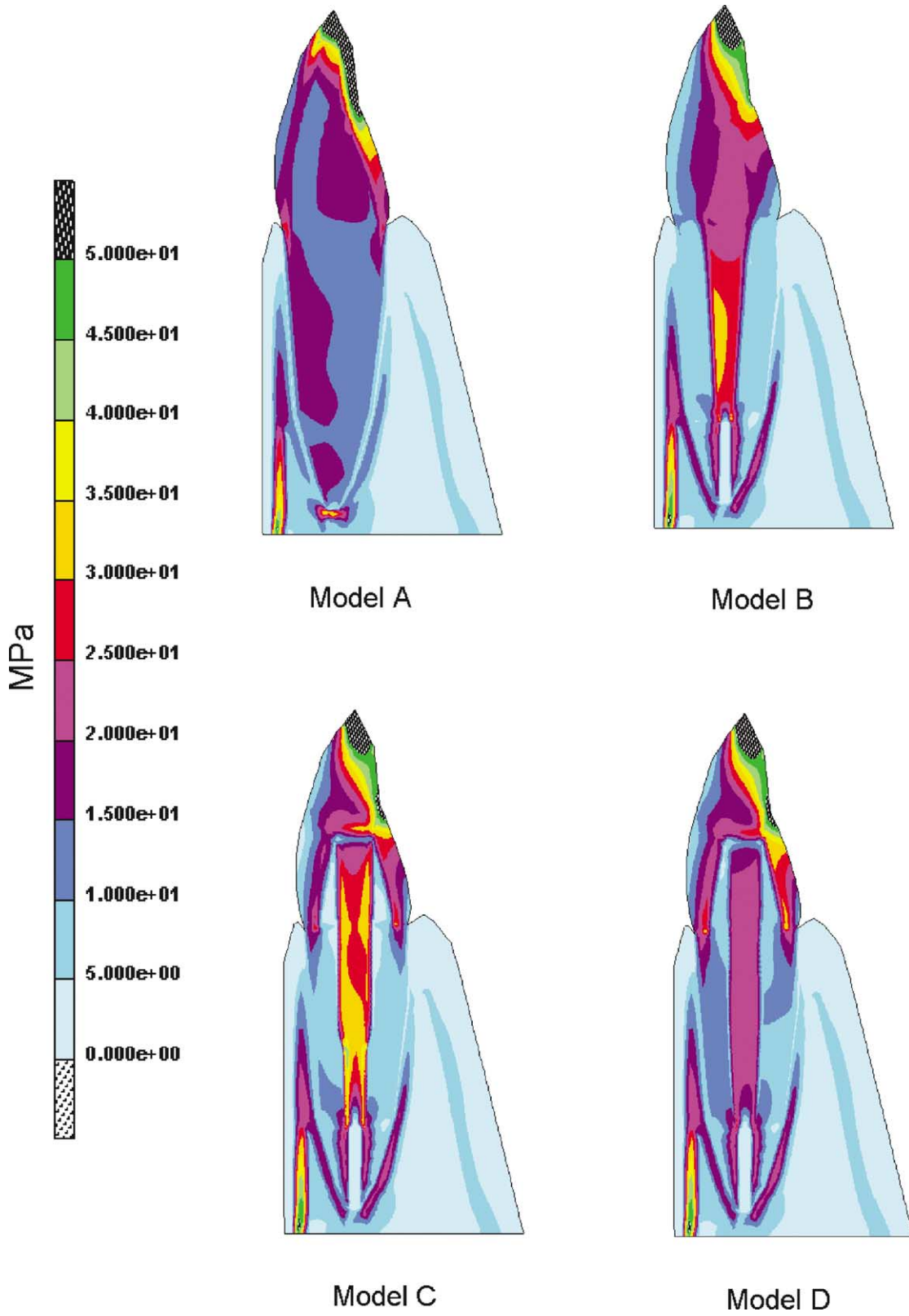


Fig. 5. Contour maps of the Von Mises stress in the case of a vertical 100 N applied load (P1).

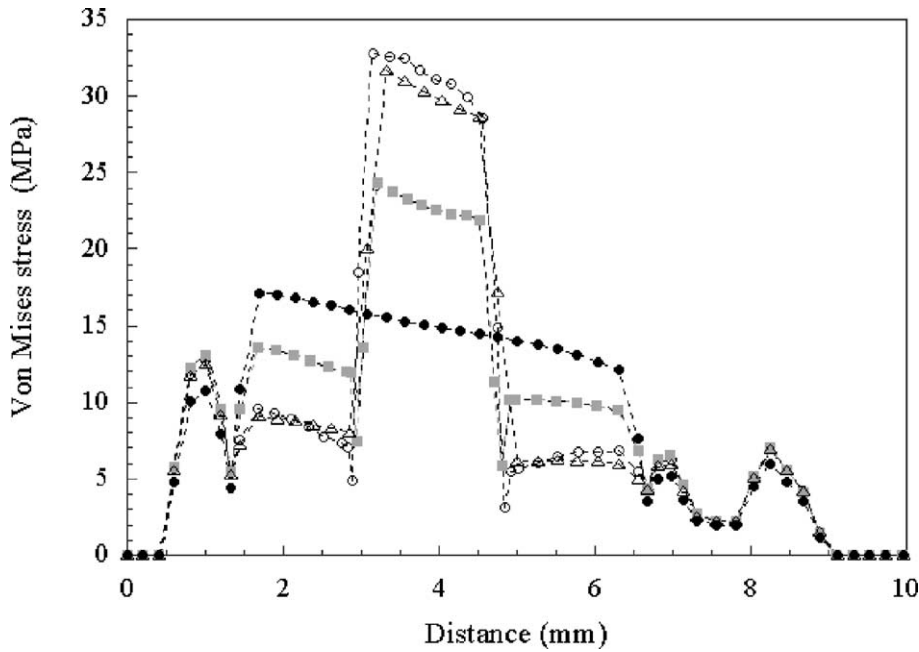


Fig. 6. Path plots on a model cross-section of the Von Mises stress in the case of a vertical 100 N applied load (P1). Symbols refer to (●) natural tooth, (△) gold alloy post, (○) carbon fibre post, and (■) glass fibre post models.

breaks at a strain value of about 4.3%, which is related to the ultimate strain of the *E*-glass fibres.

3.2. FE analysis

Von Mises equivalent stress, σ_{VM} , and shear stress, τ_{12} , were chosen as critical parameters for evaluation of the results obtained with FE simulation. Such parameters are reported as contour band maps on the entire model (Figs. 5, 7, 9, 11 and 13), and as numerical path plots (Figs. 6, 8, 10 and 12) along the line *A–A* crossing the models around their middle, as indicated in Fig. 3. In the path plots *X*-axis represents the distance from the left side of line *A–A*: posts are located between 2.95 and 4.75 mm; dentine starts at 1.7 mm and finishes at 6.3 mm; for model C and D the cement has a thickness of 0.20 mm (that is, the cement lays between 2.75 and 2.95 mm at left and between 4.75 and 4.95 mm at right). Von Mises stress is given by the following relationship [48]:

$$\sigma_{VM} = \sqrt{\sigma_I^2 + \sigma_{II}^2 + \sigma_{III}^2 - (\sigma_I\sigma_{II} + \sigma_{II}\sigma_{III} + \sigma_{III}\sigma_I)}, \quad (2)$$

where σ_I , σ_{II} , σ_{III} are the principal stress components. Von Mises stress, which is always positive in sign and depends on the whole stress field, is a widely used parameter in mechanical design, especially for the assessment of yield criteria. In this simulation we can consider it as an indicator of the average stress level, where the higher it's the value, the higher is the

possibility of damage occurrence. Shear stress can lead to rupture of the tooth/post interface and to post detachment. Consequently, the lower the shear stress level near the interface, the lower the probability of post disruption. Maps of the stresses along direction 1 (σ_{11}) and 2 (σ_{22}) were also provided by the simulation but they are not reported in the present paper. In any case it is worth noting that, in general, stresses in direction 1 resulted to be much lower (over 10 times in some case) than those directed along direction 2.

4. Discussion

4.1. Vertical load—P1

As reported in Fig. 5, in the case of a vertical 100 N load, the more critical values of the Von Mises stresses are distributed mainly inside the post and at the interface. In particular the highest values results to be located around the middle third of the root with model D possessing the lowest stress among the post-restored models, as evidenced in the path plot of Fig. 6. In the two fibre-reinforced posts (models C and D) there is also a concentration of forces at the cervical margins of the crown. This can be due to the fact that the core material has a relatively lower elastic modulus compared to surrounding materials (ceramic crown, post and dentin). On the other hand, in the case of the gold cast post-and-core, the restoring materials have much more similar

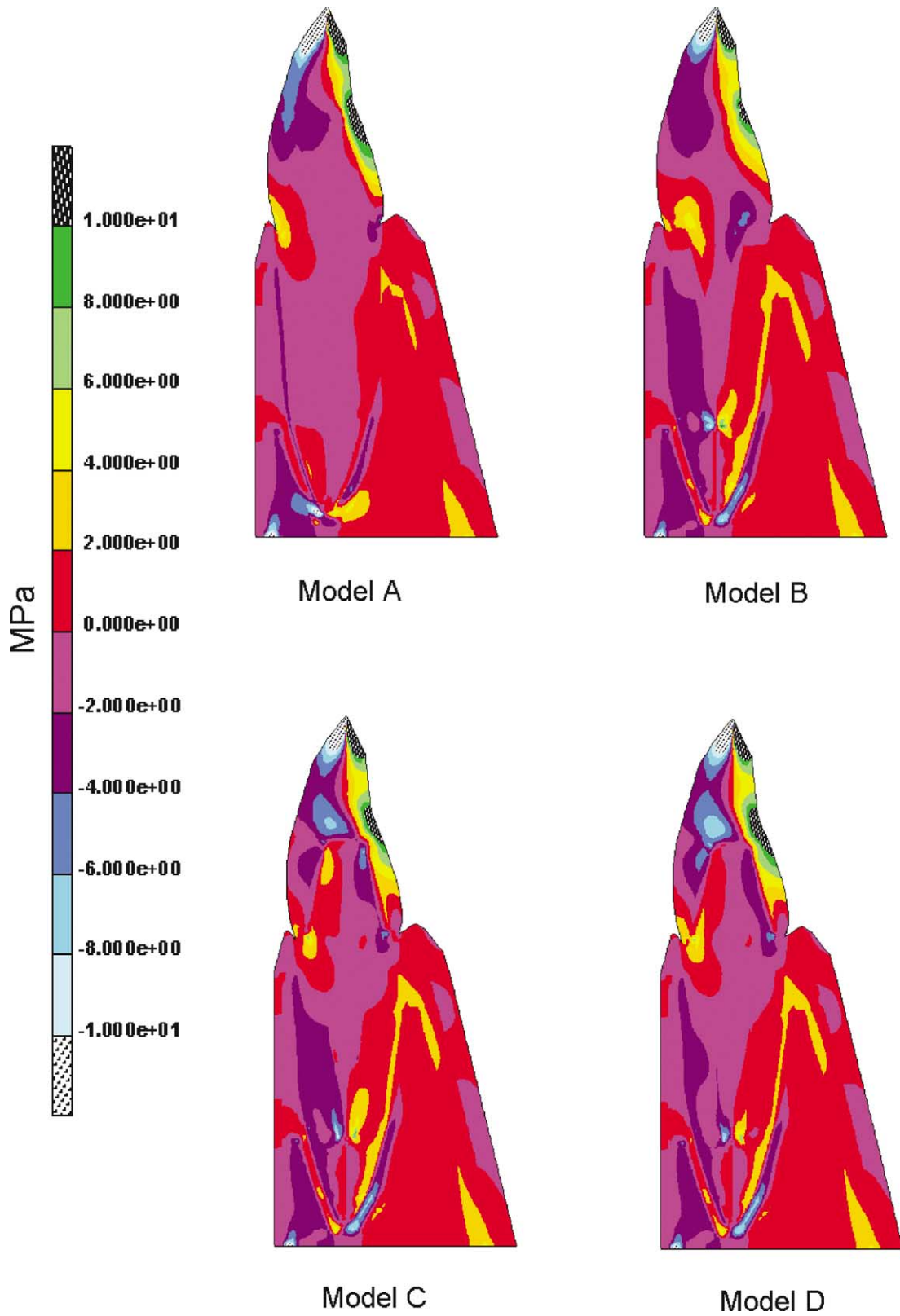


Fig. 7. Contour map of the shear stress τ_{12} in the case of a vertical 100 N applied load (P1).

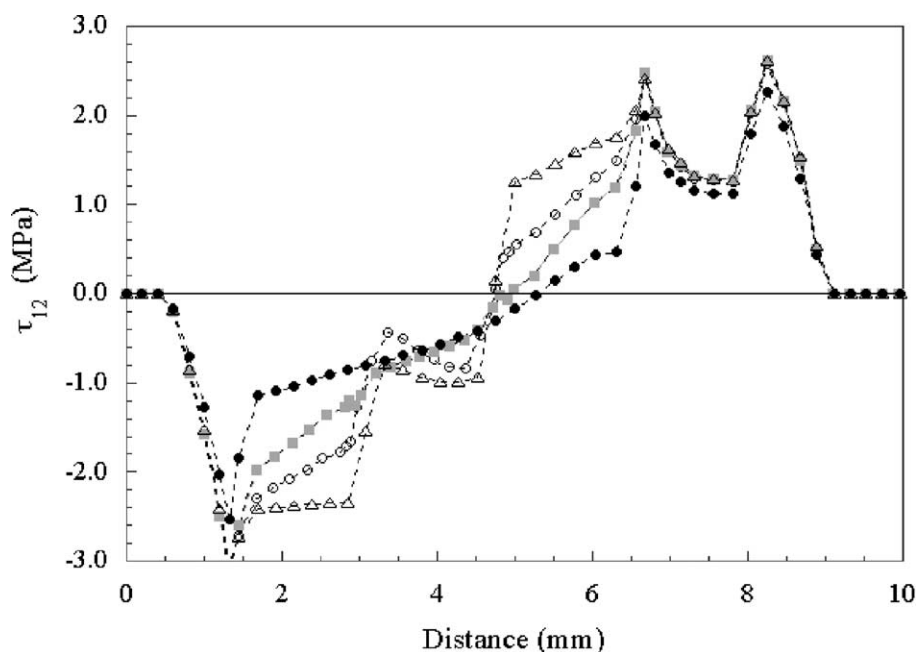


Fig. 8. Path plot along *A–A* models cross-section of the shear stress τ_{12} in the case of a vertical 100 N applied load (P1). Symbols as in Fig. 6.

stiffness and the cervical interfaces are relatively less stressed. In the case of the carbon composite post it is also evident that, a certain stress concentration arises in correspondence of the point where the post section changes.

As evidenced in Fig. 7, the maximum values of the shear stress are also located at the cervical regions and at the post apex as well. Fewer differences are found among the three post models and the peak values are of the same level as shown in Fig. 8.

4.2. Oblique load—P2

FE results regarding an oblique applied load of 50 N are reported in Figs. 9–12. Figs. 9 and 10 clearly show that a high stress concentration exists on the post surface by the coronal and middle thirds of the root on the labial side. Maximum stresses in this region are reaching about 80 MPa for models B and C, and 45 MPa for model D. It is important to note that for the glass fibre reinforced post the highest value of internal stress (about 60 MPa) lies in proximity of the outer dentin surface, which is also the case of model A. The shear stress contour map of Fig. 11 indicates the apex region of the post as possible weak point, especially in case of the gold post-and-core.

4.3. Horizontal load—P3

FE results regarding the case of a horizontal 10 N applied load are reported in Fig. 13. Horizontal load

bends the system toward the buccal direction. This is a very common case, which is one of the major causes of post crown failure. The intensity of the load condition was chosen only to observe how the systems behave to small horizontal forces. The stress fields generated in the four models are comparable to that produced in the oblique loading condition with lower stresses since applied loads are smaller. Gold post-and-core and carbon fibre prefabricated post produce the highest internal stresses, about 20 MPa, which are located on the labial side. Moreover, Fig. 13 clearly shows a concentration of forces at the cervical margin of the crown restoration where a flexible post has been used. This is clearly visible on both model C and D. Model B shows similar stress levels at the cervical margin as the natural tooth. It has to be noted that flexure of the core/post can lead to fracture failure of the post in the case of castings, or marginal gap opening and microleakage in the case of fibre-reinforced posts. On the other side, there is a higher stress concentration at the apical part in case of gold post.

The simulation under various loading directions and intensities showed that the three different posts behave differently. The gold cast post-and-core produces the greatest stress concentration at the post-dentin interface. The inherent brittleness of zinc-phosphate cement could affect the performance of this kind of restoration, eventually leading to post loosening or root fracture because of stress concentration at post apex. Fibre reinforced composite posts do also present high stress levels at the cemented interface. Anyway in this

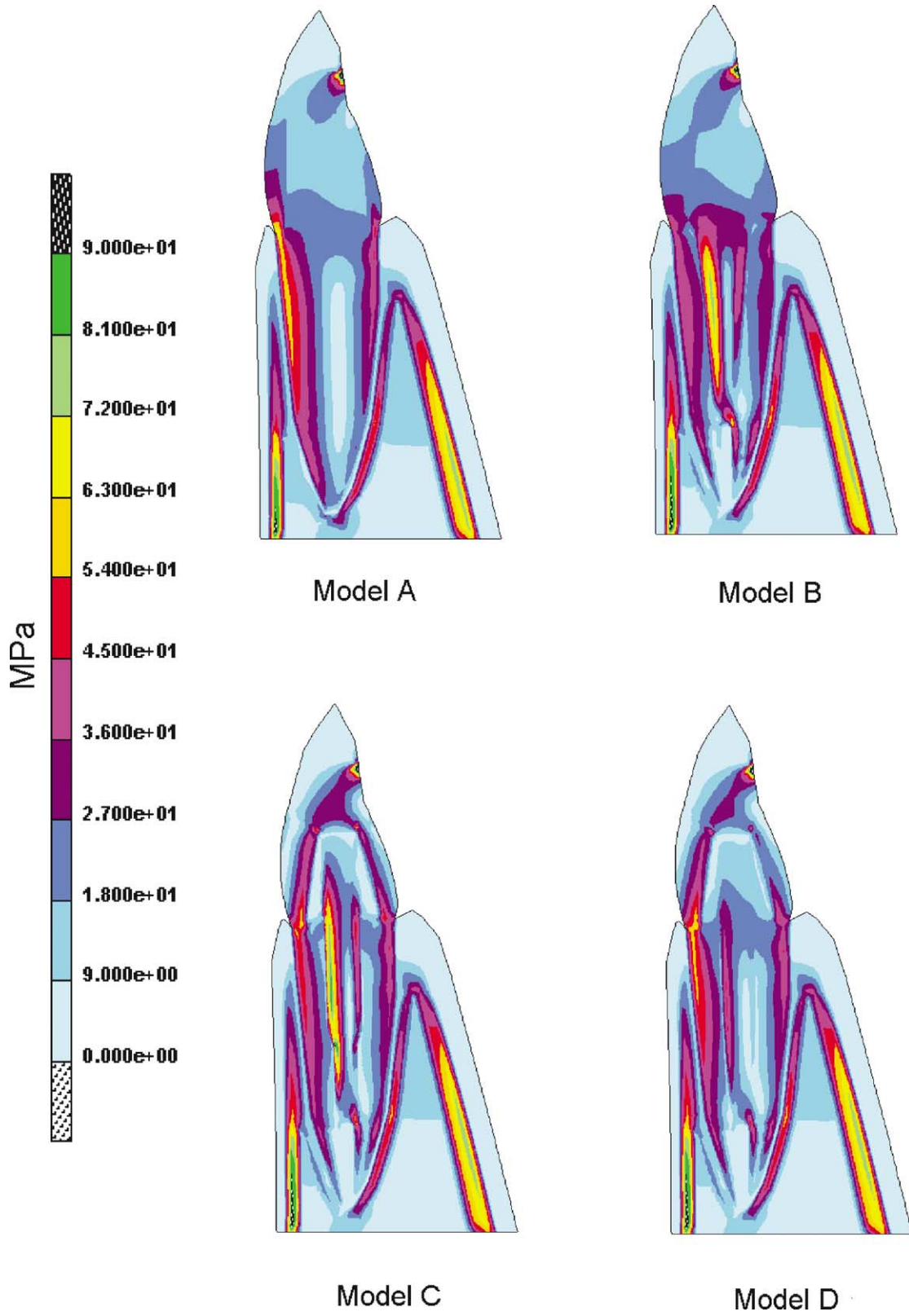


Fig. 9. Contour map of the Von Mises stress in the case of an oblique 50N applied load (P2).

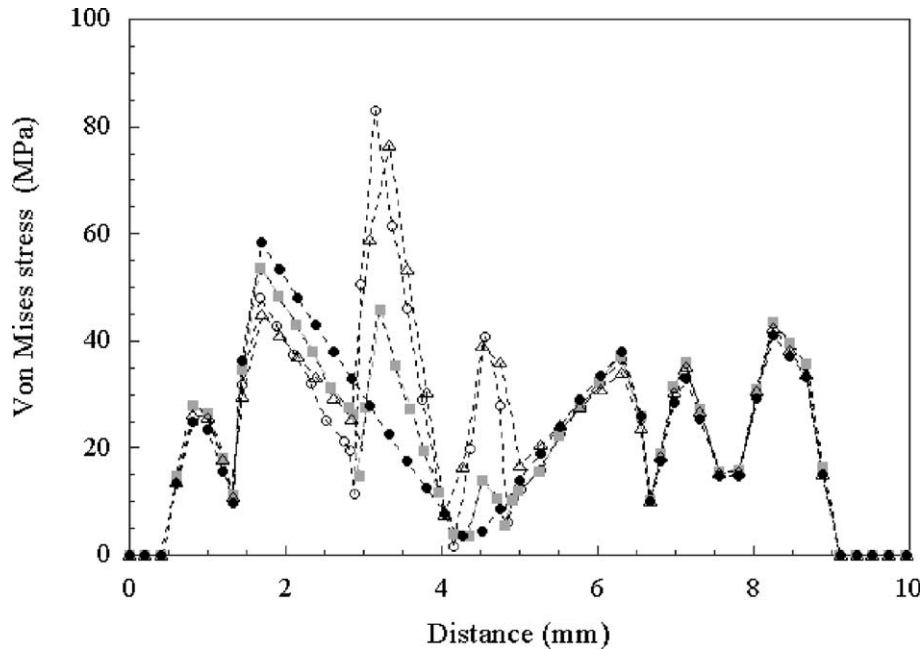


Fig. 10. Path plot along *A–A* model cross-section of the Von Mises stress in the case of an oblique 50 N applied load (P2). Symbols as in Fig. 6.

case resinous cements are used, which are stronger and possess higher bond strength, both to dentin walls and to posts. Stresses in the cervical region are also quite high for these posts, due to their flexibility and also to the presence of a less stiff core material. These could lead to microleakage or gaps at the ceramic crown interface. The glass fibre composite shows the lowest peak stresses inside the root because of a much more similar stiffness with the dentin. This limits the stresses at the post/dentine interface transferring the forces towards the external root surface. Except for the force concentration at the cervical margin, the model D resembles at most the situation of a natural tooth.

5. Conclusions

The mechanical behaviour of a new glass fibre composite post was simulated by a FE analysis on a bidimensional model. The results were compared with those obtained considering either a commercial carbon fibre post or a gold alloy cast post. A natural tooth, or better a tooth restored with ideal materials whose stiffness is equal to those of enamel and dentine, was considered as a reference model. The gold cast post-and-core produces the greatest stress concentration at the post-dentine interface. On the other hand, fibre-reinforced composite posts do present quite high stresses in the cervical region due to their flexibility and also to the presence of a less stiff core material. The glass fibre composite shows the lowest peak stresses inside the root

because its stiffness is much similar to dentin. Except for the force concentration at the cervical margin, the glass fibre composite post induces a stress field quite similar to that of the natural tooth. Stresses at the cervical margins could be lowered using less stiff crown materials, i.e. composite resins, thus obtaining an “integrated” post-core-crown system.

Appendix A

A composite material with continuous and unidirectional fibres randomly packed in the cross-section is a particular case of “orthotropic” material, called “transversely isotropic”. In general, to describe the elastic behaviour of such transversely isotropic materials five independent elastic constants are needed [49,50], i.e.: tensile longitudinal modulus E_L , transverse modulus $E_T (= E_{T'})$, shear modulus $G_{LT} (= G_{LT'})$, Poisson ratios $\nu_{LT} (= \nu_{LT'})$ and $\nu_{TT'}$, where L stands for longitudinal direction (parallel to fibre direction), and T and T' refer to two mutually perpendicular directions in the transverse plane. The minor Poisson’s ratio $\nu_{TL} (= \nu_{TL'})$ can be obtained by the following relationship:

$$\nu_{TL} = \nu_{LT} \frac{E_T}{E_L} \quad (\text{A.1})$$

while the shear modulus $G_{TT'}$ can be calculated as follows:

$$G_{TT'} = \frac{E_T}{2(1 + \nu_{TT'})} \quad (\text{A.2})$$

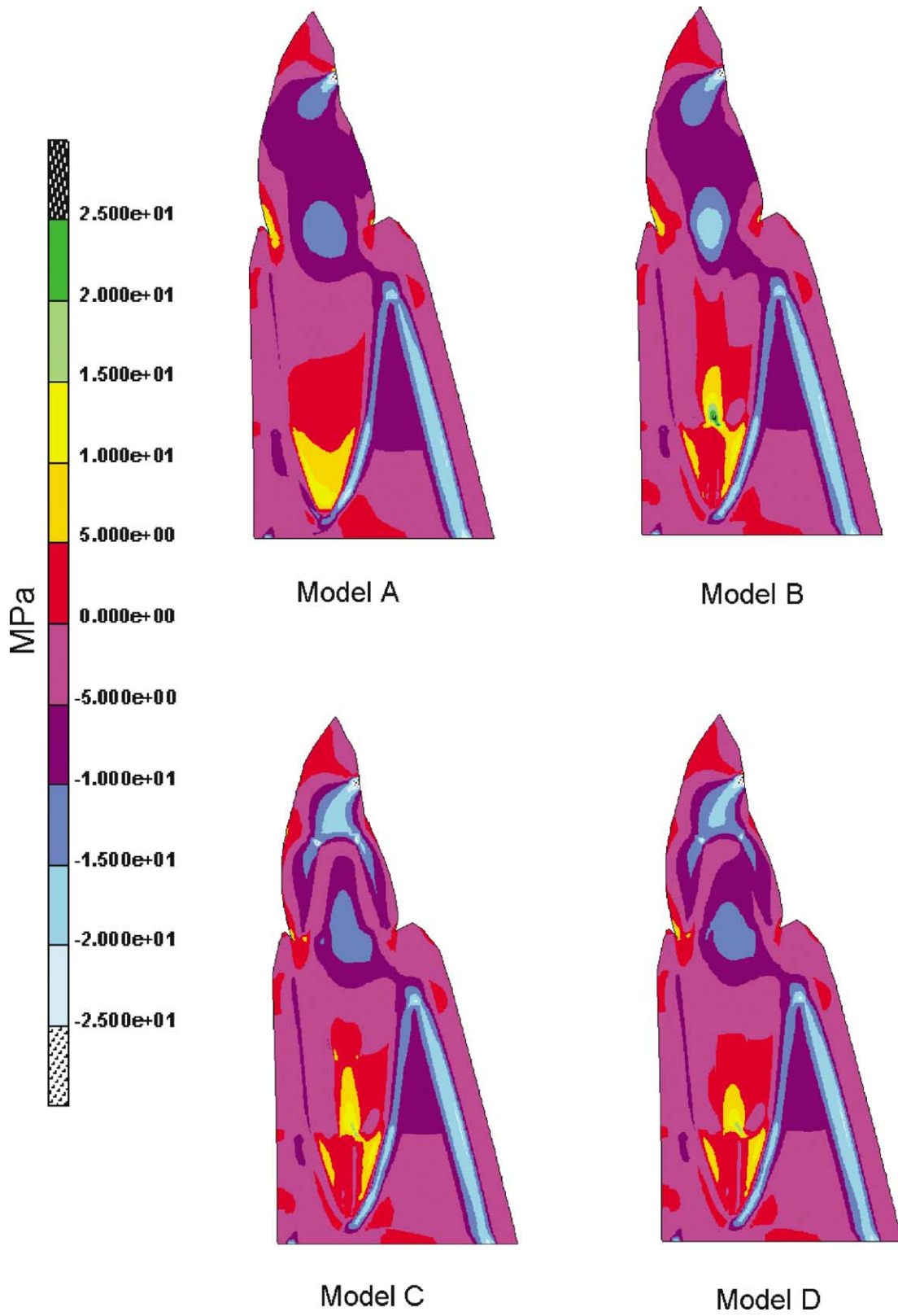


Fig. 11. Contour map of the shear stress τ_{12} in the case of an oblique 50 N applied load (P2).

The longitudinal elastic modulus of the composites material considered in FE model C was taken from literature, while in the case of model D it was experimentally determined on posts prototypes as described in the experimental section. For the estimation of the remaining four independent elastic constants, the following formulas were used (symbols f and m denote properties referred to fibre and matrix respectively; while V_f and V_m indicate their volume fractions).

The transverse elastic modulus, E_T , was taken as an average value between the estimations provided by the following Eqs. (A.3) and (A.4):

$$E_T = E_m \frac{1 + \xi \eta V_f}{1 - \eta V_f}, \tag{A.3}$$

where

$$\eta = \frac{E_f - E_m}{E_f + \xi E_m} \quad \text{and} \quad \xi = 2$$

for fibres with a round cross-section.

Tsai–Hahn equation:

$$\frac{1}{E_T} = \frac{1}{V_f + \eta V_m} \left(\frac{V_f}{E_f} + \eta \frac{V_m}{E_m} \right), \tag{A.4}$$

where $\eta = \frac{1}{2}$.

The in-plane shear modulus was taken as an average value between the estimations provided by the following equations:

Halpin–Tsai equation [41]:

$$G_{LT} = G_m \frac{1 + \xi \eta V_f}{1 - \eta V_f}, \tag{A.5}$$

where

$$\eta = \frac{G_f - G_m}{G_f + \xi G_m}$$

and $\xi = 1$ for round section fibres.

Tsai–Hahn equation:

$$\frac{1}{G_{LT}} = \frac{1}{V_f + \eta V_m} \left(\frac{V_f}{G_f} + \eta \frac{V_m}{G_m} \right) \tag{A.6}$$

with

$$\eta = \frac{1}{2} \left(1 + \frac{G_m}{G_f} \right).$$

The Poisson’s coefficient ν_{LT} was evaluated by the rule of mixture:

$$\nu_{LT} = \nu_f V_f + \nu_m V_m. \tag{A.7}$$

The Poisson’s coefficient $\nu_{TT'}$ was evaluated by using the following equation proposed by Foye [51]:

$$\nu_{TT'} = \nu_f V_f + \nu_m V_m \Phi, \tag{A.8}$$

where

$$\Phi = \frac{1 + \nu_m - \nu_{LT}(E_m/E_L)}{1 - \nu_m^2 + \nu_m \nu_{LT}(E_m/E_L)}.$$

Matrix and fibre properties used to fill the above reported equations are given in Table 4. Carbon fibres were assumed as high strength type in order to obtain

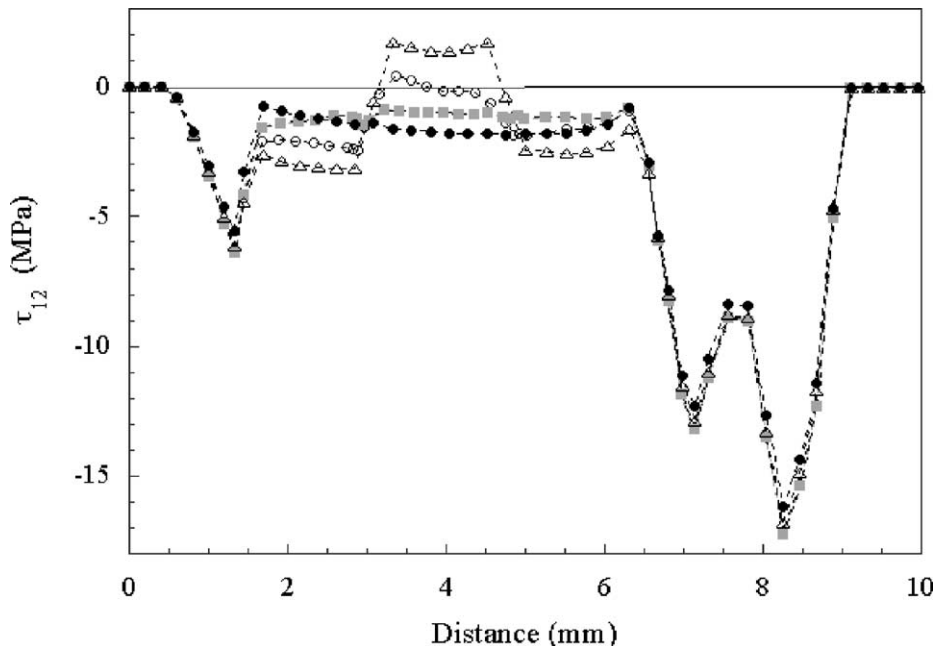


Fig. 12. Path plot along $A-A$ models cross-section of the shear stress τ_{12} in the case of an oblique 50 N applied load (P2). Symbols as in Fig. 6.

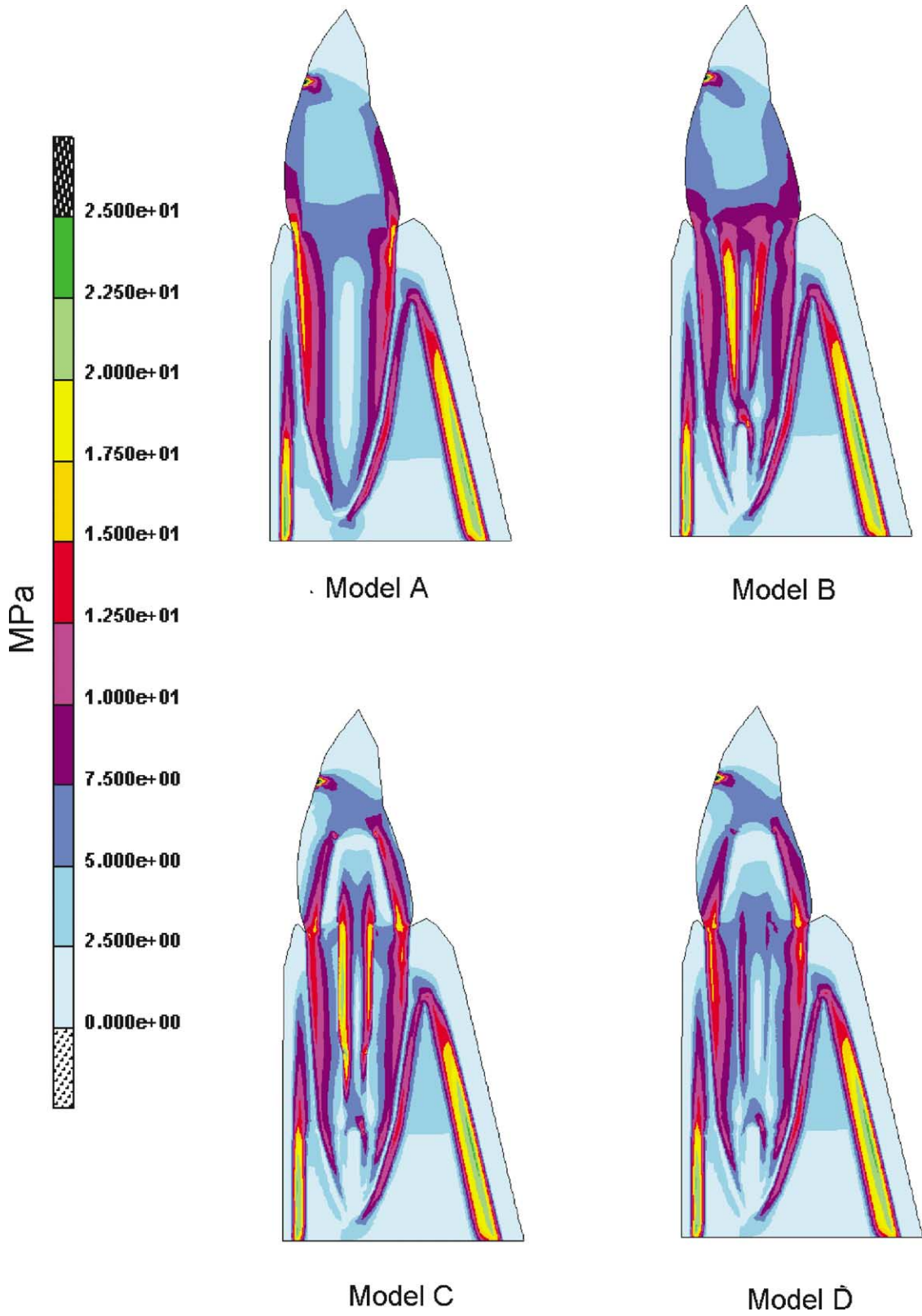


Fig. 13. Contour map of the Von Mises stress in the case of an horizontal 10N applied load (P3).

the composite properties reported in literature (i.e. $E_L = 125$ GPa and $E_T = 8.5$ GPa). Glass fibre properties are taken from the technical sheet of Hybon 2001 E-glass fibre of PPG Industries. Matrix properties are relatives to a general epoxy or acrylic resin, as found in literature [52].

References

- [1] Baraban DJ. The restoration of pulpless teeth. *Dent Clin North Am* 1967;11:633–53.
- [2] Schillenburg HT, Fisher DW, Dewhirst RB. Restoration of endodontically treated posterior teeth. *J Prosthet Dent* 1970;24:401–7.
- [3] Perel ML, Muroff FI. Clinical criteria for post and cores. *J Prosthet Dent* 1972;28:405–11.
- [4] Stern N, Hirshfeld Z. Principles of preparing endodontically treated teeth for dowel and core restoration. *J Prosthet Dent* 1973;30:162–5.
- [5] Kantor ME, Pines MS. A comparative study of restorative techniques for pulpless teeth. *J Prosthet Dent* 1977;38:405–12.
- [6] Trabert KC, Caputo AA, Abou-Rass M. Tooth fracture: a comparison of endodontic and restorative treatments. *J Endod* 1978;4:341–5.
- [7] Sokol DJ. Effective use of current core and post concepts. *J Prosthet Dent* 1984;52:231–4.
- [8] Torpe M, Maltz DO, Tronstad I. Resistance to fracture of restored endodontically treated teeth. *Endod Dent Traumatol* 1985;1:108–11.
- [9] Hunter AJ, Feiglin B, Williams JF. Effects of post placement on endodontically treated teeth. *J Prosthet Dent* 1989;62:166–72.
- [10] Phillips R. *Skinner's science of dental materials*, 8th ed. Philadelphia, PA, USA: W.B. Saunders Co., 1982.
- [11] Vallittu PK. A review of fiber-reinforced denture base resins. *J Prosthodont* 1996;5:270–6.
- [12] Reynaud M, Reynaud P, Duret F, Duret B. 1994 US Patent no. 5,328,372.
- [13] Duret B, Reynaud M, Duret F. Un Nouveau Concept de Reconstitution Coronaradiculaire: le composipost. I. Le Chirurgien-Dentist de France 1990;540:131.
- [14] Duret B, Reynaud M, Duret F. Un Nouveau Concept de Reconstitution Coronaradiculaire: le composipost. II. Le Chirurgien-Dentist de France 1990;542:69.
- [15] Freedman G. The carbon fibre post: metal-free, post-endodontic rehabilitation. *Oral Health* 1996;86(2):29–30.
- [16] Sidoli GE, King PA, Setchell DJ. An in vitro evaluation of a carbon fiber-based and core system. *J Prosthet Dent* 1997;78(1):5–9.
- [17] Torbjörner A, Karlsson S, Syverud M, Hensten-Pettersen A. Carbon fiber reinforced root canal posts. Mechanical and cytotoxic properties. *Eur J Oral Sci* 1996;104(5–6):605–11.
- [18] Fredriksson M, Astbäck J, Pamenius M, Arvidson K. A retrospective study of 236 patients with teeth restored by carbon fiber-reinforced epoxy resin posts. *J Prosthet Dent* 1998;80(2):151–7.
- [19] Karna JC. A fiber composite laminate endodontic post and core. *Am J Dent* 1996;9(5):230–2.
- [20] Burgess JO, Summitt JB, Robbins JW. The resistance to tensile, compression and torsional forces provided by four post systems. *J Prosthet Dent* 1992;68(6):899–903.
- [21] Asmussen E, Peutzfeldt A, Heitmann T. Stiffness, elastic limit and strength of newer types of endodontic posts. *J Dent* 1999;27(4):275–8.
- [22] Lambjerg-Hansen H, Asmussen E. Mechanical properties of endodontic posts. *J Oral Rehabil* 1997;24(12):882–7.
- [23] Standlee JP, Caputo AA, Collard EW, Pollack MH. Analysis of stress distribution in endodontic posts. *Oral Surg* 1972;33:952–60.
- [24] Mattison GD. Photoelastic stress analysis of cast-gold endodontic posts. *J Prosthet Dent* 1982;48:407–11.
- [25] Burns DA, Krause WR, Douglas HB, Burns DR. Stress distribution surrounding endodontic posts. *J Prosthet Dent* 1990;64(4):412–8.
- [26] Farah JW, Craig RG, Sikarskie DC. Photoelastic and finite element stress analysis of a restored axisymmetric first molar. *J Biomech* 1973;6:511–20.
- [27] Thresher RW, Saito GE. The stress analysis of human teeth. *J Biomech* 1973;6:443–9.
- [28] Davy DT, Dilley GL, Krejci RF. Determination of stress patterns in root-filled teeth incorporating various dowels design. *J Dent Res* 1981;60:1301–10.
- [29] Reinhardt RA, Krejci RF, Pao YC, Stannard JG. Dentin stresses in post-reconstructed teeth with diminishing bone support. *J Dent Res* 1983;62:1002–8.
- [30] Williams KR, Edmundson JT. A finite element stress analysis of an endodontically restored tooth. *Eng Med* 1984;13(4):167–73.
- [31] Williams KR, Edmundson JT, Rees JS. Finite element analysis of restored teeth. *Dent Mater* 1987;3:200–6.
- [32] Pao YC, Reinhardt RA, Krejci RF. Root stresses with tapered-end post design in periodontally compromised teeth. *J Prosthet Dent* 1987;57:281–6.
- [33] Ko C, Chu C, Chung K, Lee M. Effects of posts on dentin stress distribution in pulpless teeth. *J Prosthet Dent* 1992;68:421–7.
- [34] Cailleteau JG, Rieger MR, Ed Akin J. A comparison of intracanal stresses in a post-restored tooth utilizing the finite element method. *J Endod* 1992;18(11):540–4.
- [35] Huysmans MCDNJM, Vandervorst PGT. Finite-element analysis of quasi-static and fatigue failure of post and cores. *J Dent* 1993;21(1):57–64.
- [36] Ho M-H, Lee S-Y, Chen H-H, Lee M-C. Three-dimensional finite element analysis of the effects of posts on stress distribution in dentin. *J Prosthet Dent* 1994;72(4):367–72.
- [37] Yaman SD, Alacam T, Yaman Y. Analysis of stress distribution in a maxillary central incisor subjected to various post and core applications. *J Endod* 1998;24(2):107–11.
- [38] Cavalli G, Bertani P, Generali P. Finite element stress analysis in post and crown restored teeth. *G It Endo* 1996;3:107–12.
- [39] Holmes DC, Diaz Arnold AM, Leary JM. Influence of post dimension on stress distribution in dentin. *J Prosthet Dent* 1996;75(2):140–7.
- [40] Silver-Thorn MB, Joyce TP. Finite element analysis of anterior tooth root stresses developed during endodontic treatment. *J Biomech Eng* 1999;121(1):108–15.
- [41] Ukon S, Moroi H, Okimoto K, Fujita M, Ishikawa M, Terada Y, Satoh H. Influence of different elastic moduli of dowel and core on stress distribution in root. *Dent Mater J* 2000;19(1):50–64.
- [42] Zienkiewicz OC. *The finite element method*. London UK: McGraw-Hill, 1986.
- [43] Zappini G, Pegoretti A, Bianchetti M, Fambri L. New endodontic post in composite material. In *Proceedings of International Conference on Advances in Biomaterials and Tissue Engineering*, Capri, Italy, June 14–19, 1998, p. 33.
- [44] Craig RG. *Restorative dental materials*, 8th ed. St. Louis (MI) USA: CV Mosby, 1989.
- [45] Rodford RA, Braden M, Clarke RL. Variation of Young's modulus with the test specimen's aspect ratio. *Biomaterials* 1993;14(10):781–6.

- [46] Ramfjord S, Ash M. Occlusion, 3rd ed. Philadelphia (PA) USA: W.B. Saunders Co., 1983.
- [47] McCullough RL. Introduction to anisotropic elasticity. In: Carlsson LA, Gillespie JW, editors. Delaware composites design encyclopedia., vol. 2. Lancaster (PA) USA: Technomic Publishers Co., 1990.
- [48] Fenner RT. Engineering elasticity. Application of numerical and analytical techniques. Chichester UK: Ellis Horwood Ltd., 1986. p. 234–5.
- [49] Agarwal BG, Broutmann LJ. Analysis and performance of fiber composites, 2nd ed. New York: Wiley, 1990.
- [50] Tsai WS, Hahn HT. Introduction to composite materials. Lancaster (PA) USA: Technomic Publishers Co., 1980.
- [51] Foye RL. The transverse Poisson's ratio of composites. *J Comp Mater* 1972;6:293.
- [52] Penn LS, Chiao TT. Epoxy resins. In: Lubin G, editor. Handbook of composites. New York: Van Nostrand Reinhold Company Inc., 1982. p. 57–88.